

Geophysical Research Letters[®]



RESEARCH LETTER

10.1029/2023GL106172

Stronger Oceanic CO₂ Sink in Eddy-Resolving Simulations of Global Warming

Damien Couespel¹ , Marina Lévy² , and Laurent Bopp³

¹NORCE Norwegian Research Centre, Bjerknes Centre for Climate Research, Bergen, Norway, ²Sorbonne Université, LOCEAN-IPSL, CNRS/IRD/MNHN, Paris, France, ³LMD-IPSL, École Normale Supérieure/PSL University, CNRS, École Polytechnique, Sorbonne Université, Paris, France

Key Points:

- We conducted idealized ocean simulations under global warming and rising atmospheric CO₂ at coarse and eddy-resolving resolutions
- CO₂ sink is larger by 34% at eddy resolution, due to larger anthropogenic CO₂ uptake combined with weaker climate feedback
- This ensues from the model's overturning circulation sensitivity to resolution in both historical and future state

Supporting Information:

Supporting Information may be found in the online version of this article.

Correspondence to:

D. Couespel,
daco@norceresearch.no

Citation:

Couespel, D., Lévy, M., & Bopp, L. (2024). Stronger oceanic CO₂ sink in eddy-resolving simulations of global warming. *Geophysical Research Letters*, 51, e2023GL106172. <https://doi.org/10.1029/2023GL106172>

Received 10 SEP 2023

Accepted 11 JAN 2024

Author Contributions:

Conceptualization: Marina Lévy
Funding acquisition: Marina Lévy, Laurent Bopp
Investigation: Damien Couespel
Methodology: Damien Couespel, Marina Lévy
Supervision: Marina Lévy, Laurent Bopp
Visualization: Damien Couespel
Writing – original draft: Damien Couespel
Writing – review & editing: Damien Couespel, Marina Lévy, Laurent Bopp

Abstract Accurately representing the ocean carbon cycle in Earth System Models (ESMs) is essential to understanding the oceanic CO₂ sink evolution under CO₂ emissions and global warming. A key uncertainty arises from the ESM's inability to explicitly represent mesoscale eddies. To address this limitation, we conduct eddy-resolving experiments of CO₂ uptake under global warming in an idealized mid-latitude ocean model. In comparison with similar experiments at coarser resolution, we show that the CO₂ sink is 34% larger in the eddy-resolving experiments. 80% of the increase stems from a more efficient anthropogenic CO₂ uptake due to a stronger Meridional Overturning circulation (MOC). The remainder results from a weaker reduction in CO₂ uptake associated to a weaker MOC decline under global warming. Although being only a fraction of the overall response to climate change, these results emphasize the importance of an accurate representation of small-scale ocean processes to better constrain the CO₂ sink.

Plain Language Summary Today, the ocean absorbs ~25% of the CO₂ emissions caused by human activities. This CO₂ sink is primarily driven by the increase of CO₂ in the atmosphere, but it is also influenced by physical changes in the ocean's properties. Earth System Models are used to project the future of the ocean CO₂ sink. Due to limited computational capacity, ESMs need to parameterize flows occurring at scales smaller than ~100 km, their typical horizontal grid resolution. To overcome the computational limitations, we use an ocean biogeochemical model representing an idealized North Atlantic ocean of reduced dimensions. We conduct simulations of global warming using increasingly finer horizontal resolutions (from ~100 km to ~4 km). Our findings demonstrate that the ocean CO₂ uptake is highly influenced by resolution. This sensitivity primarily stems from how the overturning circulation's mean state depends on resolution, as well as how it responds to global warming. Although our results capture only a fraction of the overall oceanic response to climate change, they emphasize the significance of accurately representing the role of small-scale ocean processes to better constrain the future evolution of ocean carbon uptake.

1. Introduction

Understanding the ocean's capacity to mitigate or amplify human-induced climate change is essential for refining future climate projections, particularly for estimating the remaining carbon budget (Canadell et al., 2021). To date, the ocean absorbs ~25% of CO₂ emissions caused by human activities (Friedlingstein et al., 2022). The ocean's capacity to sequester anthropogenic CO₂ makes it a key player in determining the rate at which CO₂ accumulates in the atmosphere. Thus an important question is how this oceanic CO₂ sink will evolve under continuing CO₂ emissions and global warming, because it will influence the pace of climate change.

The strength of the oceanic CO₂ sink is set by the balance between two mechanisms. The uptake of anthropogenic CO₂ by the ocean is primarily a chemical response to the rise in atmospheric CO₂ that forces a growing disequilibrium of the partial pressure of CO₂ (pCO₂) at the air-sea interface. The carbon-concentration feedback parameter is a metric commonly used to measure how much anthropogenic CO₂ is absorbed by the ocean for each additional unit of CO₂ (expressed in ppm) added to the atmosphere, assuming the ocean dynamical and thermodynamical state remains unchanged (Arora et al., 2020; Boer & Arora, 2013; Friedlingstein et al., 2006; Katavouta & Williams, 2021; Roy et al., 2011; Schwinger et al., 2014). However, rising atmospheric CO₂ also lead to global warming, which modifies the ocean's state. Particularly the warming of surface waters and the increased ocean stratification associated with it both tend to slow down the carbon cycle, leading to a net outgassing of natural carbon and a reduced uptake of anthropogenic carbon at the global scale. This negative carbon-climate feedback

© 2024. The Authors.

This is an open access article under the terms of the [Creative Commons Attribution-NonCommercial-NoDerivs License](https://creativecommons.org/licenses/by/4.0/), which permits use and distribution in any medium, provided the original work is properly cited, the use is non-commercial and no modifications or adaptations are made.

reflects the decrease of the CO₂ sink induced by each additional degree of atmospheric warming (Maier-Reimer et al., 1996; Sarmiento & Le Quéré, 1996; Sarmiento et al., 1998). The strength of these two feedback mechanisms need to be evaluated to constrain the future evolution of the net oceanic CO₂ sink. Arora et al. (2020) used 11 Earth System Models (ESMs) from the Coupled Model Intercomparison Project Phase 6 (CMIP6) and assessed that the carbon-climate feedback (evaluated to $-17.3 \pm 5.5 \text{ PgC } ^\circ\text{C}^{-1}$ in the case of an idealized climate change scenario in which atmospheric CO₂ increases by 1% every year) partly offsets the positive carbon-concentration feedback (evaluated to $0.79 \pm 0.07 \text{ PgC ppm}^{-1}$).

An important weakness of ESMs arises from their coarse resolution horizontal ocean grid (typically 100 km or coarser), which is imposed by computational constraints. In current ESMs, sub-grid scale ocean processes, which include mesoscale eddies and submesoscale flows (Hewitt et al., 2022), are not explicitly resolved and are instead incorporated with sub-grid parameterizations (Gent & McWilliams, 1990). Improvement in the performance of these parameterizations has led to improved representation of the ocean carbon cycle and of its drivers, particularly the global net CO₂ sink over the historical period (Bronselaeer et al., 2017; Hauck et al., 2020; Séférian et al., 2020), the large-scale patterns of CO₂ uptake and outgassing, of primary production (Séférian et al., 2020), of the mixed layer depth (Fu et al., 2022; Séférian et al., 2019), and of carbon subduction/obduction (Davila et al., 2022; Lévy et al., 2013; Sallée et al., 2012). However, despite recent improvements, parameterizations still fail at capturing aspects of the model solution, particularly when it comes to biogeochemical tracers (Ruan et al., 2023). Explicitly resolving eddies in ocean models instead of parameterizing them is known to better redistribute energy transfers between scales and affect large-scale patterns of the ocean circulation; this affects the positioning of western boundary currents (Chassignet & Marshall, 2008; Chassignet & Xu, 2017; Lévy et al., 2010), alters the Meridional Overturning Circulation's strength (MOC, Hirschi et al., 2020; Roberts et al., 2020), and increases stratification (Chanut et al., 2008; du Plessis, Swart, Ansong, & Mahadevan, 2017; Karleskind et al., 2011; Lévy et al., 2010). These changes impact the transport of heat and tracers, including carbon (Chen et al., 2019; Lévy et al., 2012; Swierczek et al., 2021; Uchida et al., 2020; Uchiyama et al., 2017). Previous studies have shown the strong sensitivity of the key drivers of the ocean carbon cycle to the representation of sub-grid processes (Bahl et al., 2020; Balwada et al., 2018; Brett et al., 2023; Couespel et al., 2021; Harrison et al., 2018; Mahadevan et al., 2011; Resplandy et al., 2019). Furthermore, eddy activity may evolve with global warming (Beech et al., 2022; Martínez-Moreno et al., 2021; Oliver et al., 2015), further influencing ocean circulation and carbon transport. Investigating these effects resulting from resolved eddies has recently started within global warming scenarios (Chang et al., 2020; Hewitt et al., 2022; Rackow et al., 2022; van Westen & Dijkstra, 2021), generally using resolutions not finer than 1/10°, and to the best of our knowledge, not in terms of their implications for ocean carbon cycle feedbacks.

This study assesses the impact of explicitly representing eddies and horizontal flows with scales ranging from 10 to 100 km on the response of the oceanic CO₂ uptake, and of the carbon-concentration and carbon-climate feedback parameters, to increasing CO₂ and global warming in an ocean model. This modeling study focuses on an idealized double-gyre configuration intended to represent key aspects of North Atlantic circulation following the work of Lévy et al. (2010) and Couespel et al. (2021). The subsequent section outlines the idealized setup employed in this study, followed by the presentation of results and concluding with a discussion regarding the implications for climate projections using ESMs.

2. Methods

2.1. Model Configurations

Ocean physics were simulated with the primitive-equation ocean model NEMO (Madec et al., 2017) coupled to the biogeochemical model LOBSTER (Lévy et al., 2005, 2012), which includes explicit representation of the ocean carbon cycle (Section S1 and Table S2 in Supporting Information S1). The domain is a closed square basin on a mid-latitude (20–50°N) β -plan. It is 3,180 km wide and long and 4 km deep, bounded by vertical walls and a flat bottom with free slip boundary conditions. A double-gyre circulation is set up by analytical zonal forcings (wind stress, net heat flux and freshwater flux) which vary seasonally between winter and summer extrema. The net heat flux comprises a restoration toward a zonal atmospheric temperature profile (Figure 1 in Couespel et al., 2021) and a solar radiation allowed to penetrate within the water column. CO₂ is exchanged with the atmosphere following Wanninkhof (1992, Equation 8) and forced with a prescribed atmospheric partial pCO₂.

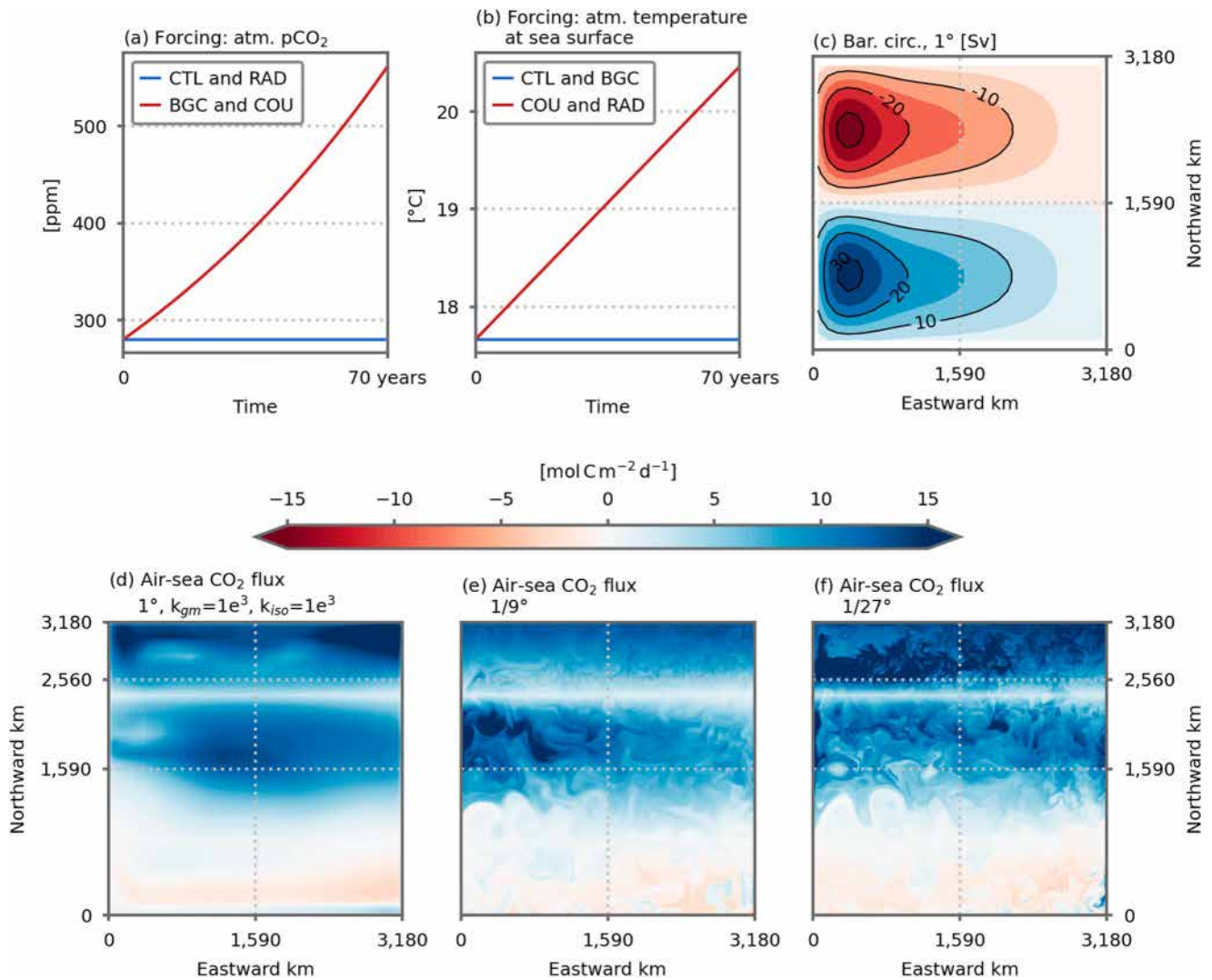


Figure 1. Overview of the model configurations and simulations. (a) Time series of the analytical atmospheric pressure of CO₂ [ppm] forcing for the CTL and RAD simulation (blue line) and for the BGC and COU simulations (red line). (b) Time series of the mean analytical atmospheric temperature [°C] forcing for the CTL and BGC simulations (blue line) and for the RAD and COU simulations (red line). Shown is the atmospheric temperature average yearly and on the domain. (c) Barotropic circulation [Sv] over the model domain (average of the five 1° resolution CTL simulations). Air-sea carbon flux [mol C m⁻² d⁻¹] on March, 3rd in (d) the 1° ($k_{gm} = 1e^3$ and $k_{iso} = 1e^3$), (e) the 1/9° and (f) the 1/27° CTL simulations. Positive values indicate a flux toward the ocean.

We compared model results over an ensemble of model configurations. We used three horizontal resolutions: 106 km (1°), 12 km (1/9°) and 4 km (1/27°). For each resolution, time steps, numerical schemes and isopycnal/horizontal diffusion were adapted (Table S1 in Supporting Information S1). For the 1° resolution configurations, we used the Gent and McWilliams (1990, GM hereafter) eddy parameterization. This parameterization relies on two coefficients, an isopycnal diffusion coefficient (k_{iso}) (also often referred to as the Redi coefficient) and a GM coefficient (k_{gm}). In order to test the sensitivity of the results to the GM parameterization, we compared five combinations of the isopycnal diffusion and GM coefficients: (a) 500 m²s⁻¹, (b) 1,000 m²s⁻¹ and (c) 2,000 m²s⁻¹ for both parameters and (d) 500 m²s⁻¹ and (e) 2,000 m²s⁻¹ for the isopycnal diffusion parameter but keeping the GM coefficient at 1,000 m²s⁻¹. We thus ended up with seven different configurations: five eddy-parameterized at a coarse resolution (1°) and two eddy-resolving at fine resolutions (1/9° and 1/27°). In the following, results from the eddy-parameterized coarse resolution configurations are synthesized by showing the average ± 1 standard deviation across the five different configurations. For the higher resolution configurations, there is no momentum nor tracer diffusion but a minimal bi-Laplacian tracer diffusion at 1/27°. Contrary to the 1/27° configuration, the qualifier "eddy-permitting" is probably more appropriate for the 1/9° configuration. Nevertheless, to simplify

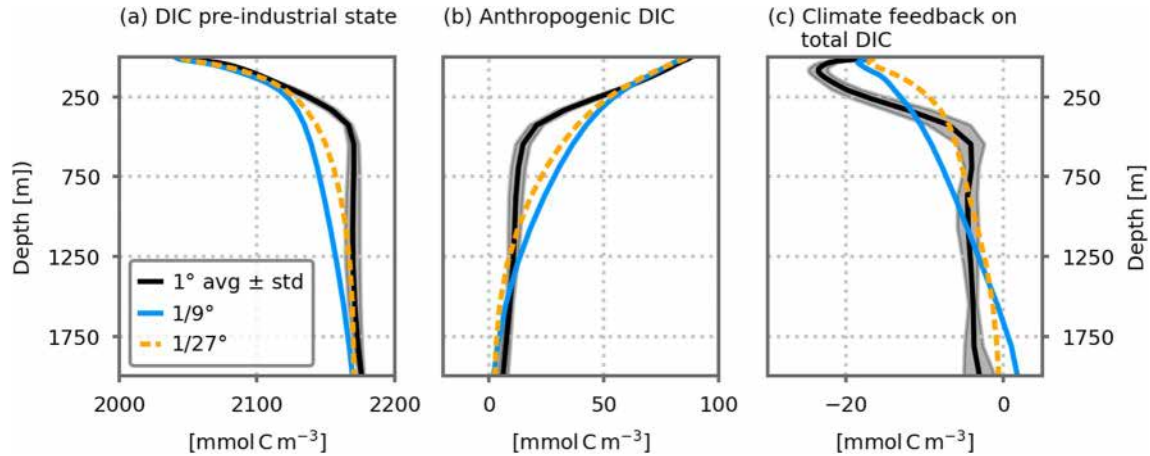


Figure 2. Dissolved inorganic carbon (DIC, mmol C m^{-3}) vertical profiles spatially averaged over the entire domain for the three resolutions. (a) DIC pre-industrial state: profiles in the CTL simulation. (b) Anthropogenic DIC: change in DIC between the BGC and CTL simulations and (c) Climate feedback on total (natural and anthropogenic) DIC: change in DIC between the COU and BGC simulations. All profiles are averaged over the 10 last years of the simulations. The 1° resolution profiles shows the average of the five 1° configurations. Shading indicates ± 1 inter-model standard deviation.

and as the emphasis is put on the differences between the 1° resolution and the finer ones, we use the term eddy-resolving for both.

The model and configurations are similar to the one described in Couespel et al. (2021) and were derived from prior studies (Kr meur et al., 2009; L vy et al., 2012; Resplandy et al., 2019). The key elements have been outlined above. For further details, we refer to the aforementioned papers.

2.2. Pre-Industrial States

Starting from a physical and biogeochemical state obtained after a 2000 years spin-up at coarse resolution, a 100 years spin-up was conducted for each model configuration, that is, for each resolution and associated parameters. The spin-up was performed under pre-industrial forcing, that is, a steady seasonal cycle for wind and atmospheric temperatures, and constant atmospheric $p\text{CO}_2$. With this strategy, the pre-industrial state obtained after the spin-up is different for each configuration and represents the equilibrated control state associated with the given set of resolution and associated parameter. This strategy is consistent with the fact that shaping different pre-industrial states is part of the effect of resolution.

The main features of the model's pre-industrial solution comprise a western boundary current (Figure II.11 in Couespel, 2018) separating a subtropical gyre outgassing carbon in the south of the domain from a subpolar gyre uptaking carbon in the north (Figures 1c–1f). A rather classic MOC (Figure A8 in Couespel et al. (2021)) is simulated with northward transport in the upper ocean (above ≈ 250 m), downwelling in the north and then southward transport at depth. In the northernmost part of the domain (2,560–3,180 northward km), deep convection occurs in winter with mixed layer depth reaching 1,000 m and more (Figure A9 in Couespel et al., 2021). As resolution increases, mesoscale eddies and filamentary structures emerge in the air-sea carbon flux (Figures 1d–1f). Dissolved Inorganic Carbon (DIC) concentration increases with depth (Figure 2a). With increasing resolution, vertical profiles are more homogeneous. The vertical gradients are weaker and DIC concentration are lower at 250–1,250 m. The small differences between resolutions of $1/9$ and $1/27^\circ$ are related to the sub-mesoscale processes that begin to appear at the finest resolution. We can also note that none of the eddy-parameterized configurations has achieved a pre-industrial state that comes close to the eddy-resolving configurations (e.g., Figure 2a). The equilibrium states have been further described in Couespel et al. (2021) and in L vy et al. (2010, 2012) though in a slightly different set-up.

2.3. Set of Model Experiments

After the spin-up, four different experiments are conducted in order to evaluate the carbon-concentration and carbon-climate feedbacks. They are forced by different combinations of atmospheric temperature and

atmospheric pCO₂ (see Figures 1a and 1b). (a) The control simulation (CTL) is the continuation of the spin-up, with temperature keeping a seasonal cycle and atmospheric pCO₂ staying constant. (b) In the biogeochemical simulation (BGC), atmospheric pCO₂ increases by 1% every year, but atmospheric temperature stays constant (with a seasonal cycle). (c) In the radiative simulation (RAD), atmospheric temperature increases by 0.04°C every year (with a seasonal cycle), while atmospheric pCO₂ is kept constant. (d) In the coupled simulation (COU), both atmospheric pCO₂ and atmospheric temperature increase by 1% and 0.04°C every year, respectively. The term coupled (COU) is to be coherent with the naming used with ESMs. However, here, atmospheric temperature and atmospheric pCO₂ are not radiatively coupled. Besides, despite the use of the term "atmospheric," there is no atmospheric model. 0.04°C/year of warming is within the range of warming simulated by the ESMs forced with the atmospheric CO₂ increasing by 1% every year (Arora et al., 2020).

Following (Arora et al., 2020), the carbon-concentration and carbon-climate feedbacks are defined as:

$$\text{carbon-concentration feedback: } \beta = \frac{\Delta C_{BGC}}{\Delta C_{atm}} \quad (1)$$

$$\text{carbon-climate feedback: } \gamma = \frac{\Delta C_{COU} - \Delta C_{BGC}}{\Delta T_{atm}} \quad (2)$$

where ΔC_{BGC} and ΔC_{COU} are the cumulative change in carbon uptake in the BGC or COU simulations relative to the CTL simulation, ΔC_{atm} is the accumulation of CO₂ in the atmosphere and ΔT_{atm} is the change in atmospheric temperature.

2.4. DIC Budget

In order to provide further insights on the drivers of the carbon-concentration and carbon-climate feedbacks, we examine the DIC budgets in the different simulations. The anthropogenic DIC distribution and budget is evaluated as the difference between the BGC and the CTL simulations. The differences between the RAD and CTL simulations enables us to evaluate the response of natural DIC to warming-induced changes (Figure S2a in Supporting Information S1). The difference between the COU and BGC simulations includes both the response of natural DIC to warming and of anthropogenic DIC to warming-induced changes (Figure S2b in Supporting Information S1).

Locally, the DIC budget can be expressed as: $-\vec{\nabla} \cdot (\vec{u} \cdot DIC) + \partial_z(k \cdot \partial_z DIC) + L(DIC) + B(DIC) + fCO_2 = \partial_t DIC$. $\vec{\nabla} \cdot (\vec{u} \cdot DIC)$ is the divergence of the advective fluxes, $\partial_z(k \cdot \partial_z DIC)$ is the vertical diffusion term, $L(DIC)$ is the isopycnal diffusion, $B(DIC)$ represents the biological sources and sinks of DIC and fCO_2 the air-sea CO₂ flux when at the surface. u is the total velocity and includes the bolus velocity of the GM parametrization at coarse resolution. Integrated on the upper ocean (surface to 250 m depth) and along the 70 years of the simulations, the local DIC budget becomes:

$$\begin{aligned} \text{CO}_2 \text{ uptake : } \int_0^{70} \langle fCO_2 \rangle dt &= \int_0^{70} \oint \vec{u} \cdot DIC \, ds \, dt && \text{Advection} \\ &- \int_0^{70} \langle k \cdot \partial_z DIC|_{250m} \rangle dt - \int_0^{70} \langle L(DIC) \rangle dt && \text{Diffusion} \\ &+ \int_0^{70} \langle B(DIC) \rangle dt && \text{Biological sources and sinks} \\ &+ \Delta \langle DIC \rangle && \text{Change in DIC stock} \end{aligned} \quad (3)$$

The bracket stands for the volume integral on the upper ocean or the horizontal integral at the surface for the CO₂ uptake and at 250 m depth for the vertical diffusion term. The first term on the right side is the integral of the advective fluxes entering/exiting the upper ocean, that is, the vertical DIC advective flux at 250 m depth, here. A similar budget is computed for the lower ocean (250 m depth to bottom). In that case, the CO₂ uptake by the ocean term is null. These budgets have been computed at each time step of all the simulations. Furthermore, particularly for relating the advective transport with the MOC, the budget is also computed with the upper and lower ocean

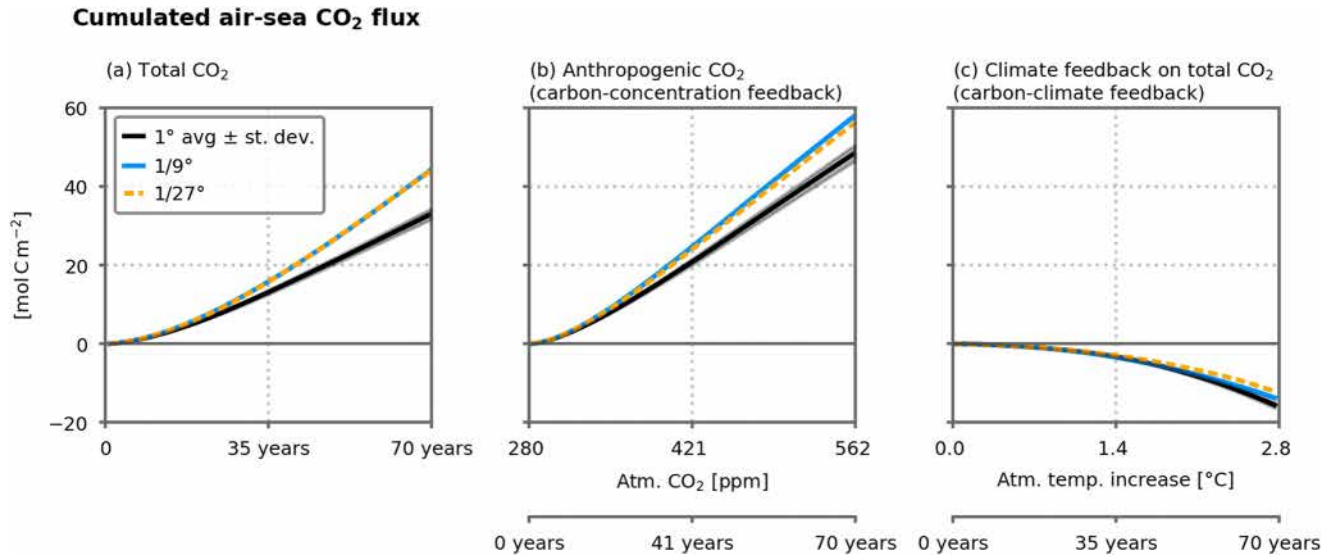


Figure 3. Time series of (a) the cumulated air-sea total (natural and anthropogenic) CO₂ flux [mol C m⁻²] for the three resolutions (COU – CTL simulations), (b) the cumulated anthropogenic CO₂ flux [mol C m⁻²] (BGC – CTL simulations) versus atmospheric pressure of CO₂ [ppm] for the three resolution and (c) the change in cumulated air-sea total CO₂ flux [mol C m⁻²] due to warming (COU – BGC simulations) versus change in atmospheric temperature [°C] in the COU simulation. The 1° resolution line shows the average of the five 1° configurations. Shading indicates ± 1 inter-model standard deviation. Positive values indicate fluxes toward the ocean.

being divided latitudinally in 3 regions representing the subtropical gyre, the subpolar gyre and the convection zone (respectively 0–1,590, 1,590–2,560 and 2,560–3,180 northward km, see Sec. S2) Because changes in DIC are not affecting biological processes (e.g., primary production) in our model, changes in biological sources and sinks of DIC only come into play in the COU and RAD simulations.

3. Results

3.1. Sensitivity of Ocean Carbon Uptake to Resolution

All along the 70 years of the COU simulation, carbon accumulates in the ocean (Figure 3a). This accumulation is driven by the rise in atmospheric pCO₂, slightly offset by the response to warming-induced changes in ocean circulation and biogeochemistry (Figures 3b and 3c). At coarse resolution, the carbon-concentration feedback is $0.18 \pm 0.01 \text{ mol C m}^{-2} \text{ ppm}^{-1}$ while the carbon-climate feedback is $-5.42 \pm 0.28 \text{ mol C m}^{-2} \text{ °C}^{-1}$. As a consequence, DIC concentration increases in the BGC simulation compared with the CTL simulation (Figure 2b), and decreases in the COU simulation compared with the BGC simulation (Figure 2c). The strongest changes take place in the first 500 m.

With finer resolution, the ocean uptakes about 34% more carbon (Figure 3a and e.g., in Figure 4, $585 - 139 = 446 \text{ Tmol C}$ at 1/9° resolution instead of $490 - 157 = 333 \text{ Tmol C}$ at 1° resolution). 84% (1/9°) and 70% (1/27°) of this extra uptake is caused by a stronger response to atmospheric pCO₂ increase (Figures 3b and e.g., in Figure 4, at 1/9° resolution, $+95 \text{ Tmol C}$ out of $446 - 333 = 113 \text{ Tmol C}$). The remainder is explained by a weaker decline in uptake because of warming (Figure 3c). The carbon-concentration feedback is stronger (0.22 and $0.21 \text{ mol C m}^{-2} \text{ ppm}^{-1}$ for the 1/9° and 1/27° resolution, respectively) while the carbon-climate feedback is weaker (-4.93 and $-4.23 \text{ mol C m}^{-2} \text{ °C}^{-1}$ for the 1/9° and 1/27° resolution, respectively). As a consequence, there is a stronger DIC concentration increase in the BGC simulation (as compared with the CTL simulation, Figure 2b), notably at subsurface (250–1,250 m).

3.2. Resolution-Induced Changes in the Carbon-Concentration Feedback

The carbon-concentration feedback depends on the ability of the ocean to transport anthropogenic carbon to the deep ocean, so that the uptake at the surface is maintained (Figures 2b and 4a). Once in the ocean, anthropogenic carbon is advected northward by the upper limb of the MOC. It is then transferred downwards (through mixing and advection) in the high latitude part of the domain (mainly the convection zone) before being advected

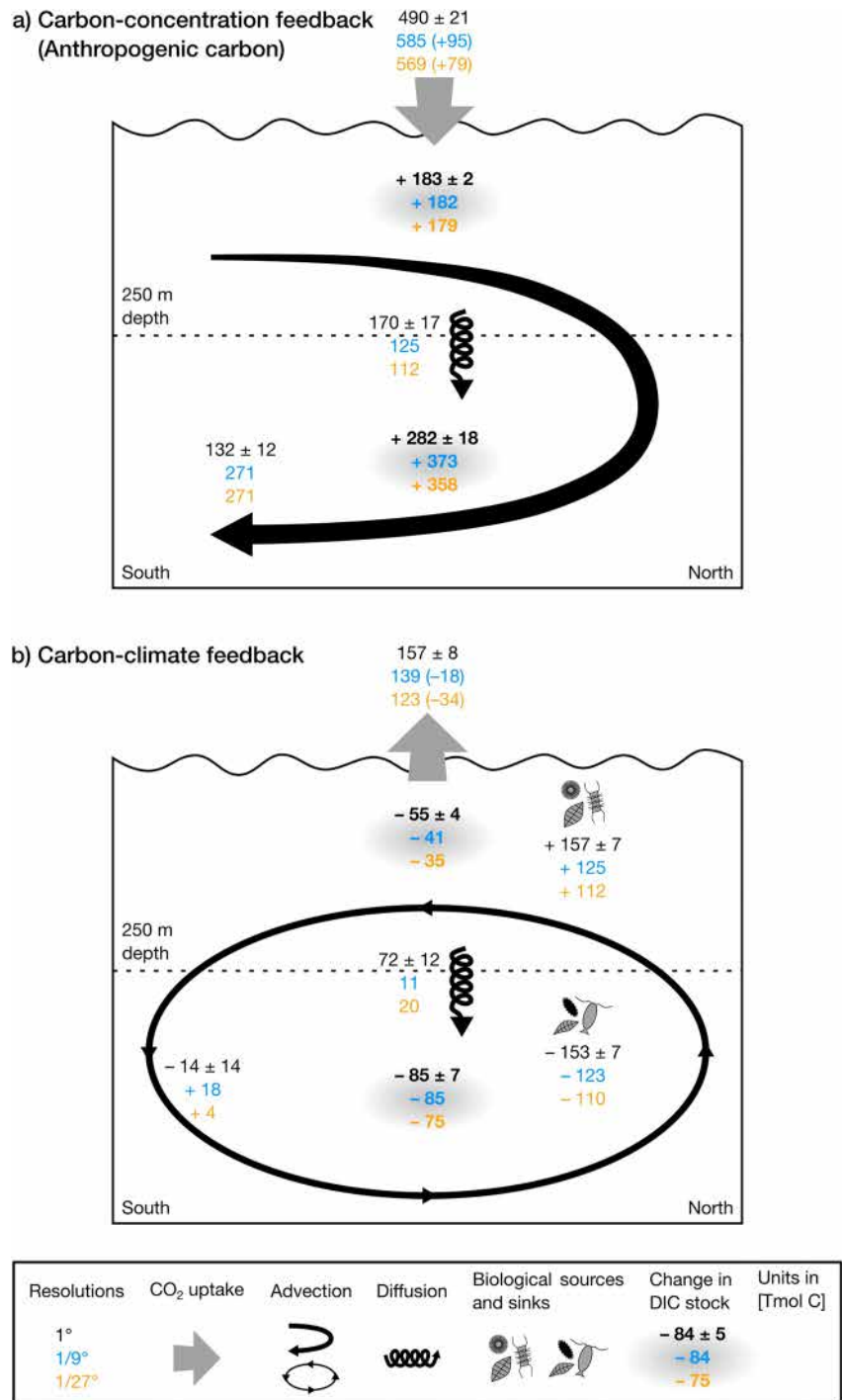


Figure 4. Anomalies in dissolved inorganic carbon (DIC) budgets and air-sea CO₂ fluxes (integrated over space and time) in the upper and lower ocean (resp. above and below 250 m depth) for the three resolutions (see Equation 3). (a) Carbon-concentration feedback (anthropogenic carbon): differences between the BGC and CTL simulations. (b) Carbon-climate feedback: differences between the COU and BGC simulations. Bold numbers stand for changes in DIC stocks. Thin number for differences in CO₂ uptake, physical transport (advection, diffusion) and the biological sources and sinks. The CO₂ uptake arrow indicate the direction of the flux (uptake or outgas); the bracketed numbers indicate the difference between the finer resolution and the coarse 1° resolution. For advection and diffusion terms, positive values stand for a DIC transport from upper to lower ocean. The arrow indicate the direction of the difference of the fluxes. For advection, it is a synthetic view of Figure S1 in Supporting Information S1. The 1° resolution numbers are the average of the five 1° configurations ± 1 inter-model standard deviation.

back southward. A small fraction is then advected upward back to the surface (Figure S1 in Supporting Information S1). Diffusive flux participates in this downward flux of carbon by counteracting against the gradients (Figure 2b). About 90% of the diffusion occurs in the convection zone.

With finer resolution, more anthropogenic carbon is transported and stored at depth (Figures 2b and 4a). Below 250 m, there is about 90 extra Tmol C stored in the finer resolution (Figure 4a), mostly in the subtropical gyre (Figure S1 in Supporting Information S1). 95–79 extra Tmol C are absorbed at the air-sea interface. This extra carbon is advected northward at the surface, downward in the convection zone and then southward to ultimately being accumulated in the sub-surface of the subtropical gyre. Advection transports more anthropogenic carbon to the sub-surface at finer resolution. This more vigorous advection is related to the stronger MOC (Couespel et al., 2021, Figure A8), MOC increasing from 1.75 Sv at 1° to 3.14 Sv at 1/9° and 2.94 Sv at 1/27°. The stronger advection is partially offset by slightly weaker vertical mixing at finer resolution, likely related to the weaker DIC gradient at finer resolution (Figure 2b).

3.3. Resolution-Induced Changes in the Climate-Carbon Feedback

The decrease in carbon uptake associated with global warming is a consequence of decreasing CO₂ solubility (induced by warming) and of the balance between changes in DIC transport, leaving more DIC at depth, and the decline in DIC consumption by primary production at the surface (Figure 4b). The major change is the decline in biological consumption of DIC at the surface (leading to $+157 \pm 7$ Tmol C at the surface), mirrored by a decline in organic matter remineralization at depth (i.e., -153 ± 7 Tmol C at depth). This results in less carbon exported to the deep ocean. It mostly happens in the subpolar gyre and the convection zone, which are also the areas with the stronger decline in primary production (Figure S1 in Supporting Information S1 and Couespel et al., 2021). The second largest change is the increase in downward diffusive fluxes transporting more carbon from the surface to the deep ocean ($+72 \pm 12$ Tmol C at depth), mostly in the convection zone (Figure S1 in Supporting Information S1). It is likely related to the shallowing of the mixed layer depth (Couespel et al., 2021, Figure A9). Changes in advection have minor impact in terms of transport between the surface and deep oceans (-14 ± 14 Tmol C at depth). However, this comes from a compensation between a strong decrease in upward and downward advective fluxes (Figure S1 in Supporting Information S1) driven by the MOC decline (Couespel et al., 2021, Figure A8). Changes in the DIC transport results from a compensation between a decline in the upward transport of natural DIC and the downward transport of anthropogenic DIC (Figure S2 in Supporting Information S1). The decrease in upward transport of natural DIC, paired with the decrease in upward transport of nutrients, is the counterpart to the decrease in biological consumption. The two almost offset each other, although more carbon is left in the deep ocean. Finally, it should be pointed out that because the model is forced toward a restoring atmospheric temperature, the warming in the surface ocean depends weakly on the resolution, thus the weak impact of resolution on the solubility change (Figure S5 in Supporting Information S1).

The climate change induced responses of DIC transport and biological source and sink of DIC are weaker at finer resolution (Figure 4b). A weaker decrease in primary production leads to a weaker decline in DIC consumption at the surface, as well as a weaker decline in remineralization at depth; that is, a weaker (by 20–28%) decline in carbon export to the deep ocean. The weaker (by 72–84%) increase in the downward diffusive flux may be related to a weaker shallowing of the mixed layer depth (Couespel et al., 2021, Figure A9). However, it should be noted that the finer resolution simulations do not include isopycnal mixing that is present in the coarse resolution simulations and added to the diffusive flux. Finally, advection changes result in more (and not less) carbon left in the deep ocean in the 1/9° and 1/27° resolution simulations. This also stems from a compensation between decreases in the upward and downward advective fluxes, although the decrease is weaker at finer resolution (Figure S1 in Supporting Information S1). This is likely related to the weaker decline in the MOC at finer resolution (Couespel et al., 2021, Figure A8). As for the coarse resolution, changes in DIC transport arise from the decline in the upward transport of natural DIC (compensating the decline in DIC consumption) and the decline in the downward transport of anthropogenic DIC (Figure S2 in Supporting Information S1).

4. Discussion and Conclusions

Using a wind and buoyancy driven double-gyre ocean biogeochemical model to perform idealized simulations of global warming, we show that the ocean carbon sink is sensitive to horizontal grid resolution. It is about 34%

larger at eddy resolution. The ocean carbon sink results from the combination of direct uptake of human emitted CO₂ (carbon-concentration feedback) as well as the negative effect induced by the carbon-cycle response to global warming (carbon-climate feedback). About 78–87% of the larger carbon uptake at high resolution results from a stronger direct uptake of anthropogenic carbon induced by a stronger transport at depth through the MOC. The remainder comes from a weaker negative carbon-climate feedback, likely related to a weaker decline in the MOC and primary production in response to warming (Figure 4 and Couespel et al., 2021).

The carbon-concentration and carbon-climate feedbacks evaluated at coarse resolution in this study are in the range of previous estimates from ESMs. In the North Atlantic, the region most similar to our idealized setting, they are respectively estimated to be about 1–10 g C m⁻²ppm⁻¹ and –50 to –300 g C m⁻²°C⁻¹ in simulations run with ESMs (Katavouta and Williams (2021, Figure 2) and Roy et al. (2011, Figure 10a and Figure 11a)). In this study, at coarse resolution, the feedbacks are respectively 2.16 ± 0.12 g C m⁻²ppm⁻¹ and -65.04 ± 3.36 g C m⁻²°C⁻¹. Although the North Atlantic is a key region (especially considering its relatively small size), the other ocean basins also contribute to the carbon-concentration and carbon-climate feedbacks and involve others drivers; for example, in the Southern Ocean, biology may have a greater role and compete with the decrease in solubility and physical ventilation (Katavouta & Williams, 2021).

In line with prior studies (Brown et al., 2021; Iudicone et al., 2016; Katavouta & Williams, 2021; Nakano et al., 2015; Ridge & McKinley, 2020), our results highlight the importance of having a reliable MOC for projecting future anthropogenic carbon uptake by the ocean. Indeed, we found that in the fine resolution simulation, the stronger MOC implies a stronger transport of anthropogenic carbon at depth and thus a stronger carbon-concentration climate feedback while a weaker MOC decline was associated with a weaker carbon-climate feedback. Such positive correlations between the pre-industrial MOC and the carbon-concentration feedback as well as between the MOC decline and the carbon-climate feedback have been identified in the latest ESMs (Katavouta & Williams, 2021), although not in previous generations (Roy et al., 2011). Our model behavior is unusual: the finer resolution simulations have a stronger carbon-concentration feedback and a weaker carbon-climate feedback, while the opposite is found in ESMs projections (Arora et al., 2020). This is likely related to the unusual behavior of the MOC in our simulations: the stronger MOC at finer resolution experiences a weaker decline, while ESMs with a stronger MOC usually project a stronger decline (Chang et al., 2020; Gregory et al., 2005; Jackson et al., 2020; Roberts et al., 2020; Winton et al., 2014). The reasons for the MOC sensitivity to resolution remains unclear in the literature (Hirschi et al., 2020); potential causes involved, for example, stronger air-sea interactions at fine resolution (Roberts et al., 2016), different spatial distributions of perturbations by the eddies (Spence et al., 2013) or the introduction of biases (Delworth et al., 2012). In the simulation used here, the stronger MOC at finer resolution is coherent with the lower stratification (thus more convection) while the weaker decline is coherent with the weaker increase in stratification (Couespel et al., 2021).

There are two areas for improvement in the MOC: its mean state and its response to global warming. Our results suggest that addressing the effect of sub-grid processes on the mean state only could largely correct for the resolution-related uncertainty in carbon uptake and induced climate feedbacks. The improved representation of the MOC can be achieved by several solutions that are currently being explored: finer resolution simulations (Chang et al., 2020; Gutjahr et al., 2019; Haarsma et al., 2016; van Westen & Dijkstra, 2021; Yeager et al., 2021), the implementation of improved parametrization schemes (Bachman, 2019; Jansen et al., 2019; Mak et al., 2018), or the use of statistical approaches (Barthélémy et al., 2022; Bolton & Zanna, 2019; Sonnewald et al., 2021; Zanna & Bolton, 2020).

In this work, we identified resolution related uncertainties in the projection of future ocean carbon uptake in an idealized regional setting. Many other features may contribute to the sensitivity of ocean carbon uptake to resolution. Changes in the MOC may also be driven by freshwater input (Jackson et al., 2020; Le Bras et al., 2021), driven by changes in wind stress pattern (Yang et al., 2020), or related to changes in adjacent regions and involving the formation of different water masses (Bronselaer et al., 2016; Delworth & Zeng, 2008; Lique & Thomas, 2018). Carbon uptake is also dependent on the biological carbon pump and the vast number of interconnected processes involved (Henson et al., 2022), whose representation varies among the models (Laufkötter et al., 2015; Séférian et al., 2020). The North Atlantic is the oceanic regime closest to our configurations, but other regions have significant contributions to the global ocean carbon cycle feedbacks (Katavouta & Williams, 2021). For example, the Southern Ocean alone accounts for 40% of the total anthropogenic carbon uptake (DeVries, 2014). The more realistic configurations and the more complex global warming scenarios developed in the CMIP6 (and subsequent

MIPs) framework would enable these different elements to be explored. The uncertainties linked to the resolution in climate models are just starting to be explored. The sensitivity of ocean carbon uptake projections to resolution raises concerns about the robustness of related climate change responses such as heat uptake and transport (Bronslaer & Zanna, 2020; Chen et al., 2019) or ocean acidification (Kwiatkowski et al., 2020).

Data Availability Statement

The data on which this article is based are available in Couespel (2023b). Due to the large volume of model output (16 TB), some of the data are available on request. The Python scripts used for analyzing the model's outputs and for producing the figures are available in Couespel (2023a).

Acknowledgments

This research was supported by the Chaire Channel at ENS. DC acknowledges the EU-funded project OceanICU (101083922). This work used high performance computer resources from GENCI-IDRIS (Grants 2016-i2016017608, 2016-A0010107608, 2018-A0040107608 and 2019-A0070107608). The authors thank Christian Ethé and Claude Talandier for helping to adapt model configuration.

References

- Arora, V. K., Katavouta, A., Williams, R. G., Jones, C. D., Brovkin, V., Friedlingstein, P., et al. (2020). Carbon-concentration and carbon-climate feedbacks in CMIP6 models and their comparison to CMIP5 models. *Biogeosciences*, 17(16), 4173–4222. <https://doi.org/10.5194/bg-17-4173-2020>
- Bachman, S. D. (2019). The GM+E closure: A framework for coupling backscatter with the Gent and McWilliams parameterization. *Ocean Modelling*, 136, 85–106. <https://doi.org/10.1016/j.ocemod.2019.02.006>
- Bahl, A., Gnanadesikan, A., & Pradal, M.-a. S. (2020). Scaling global warming impacts on ocean ecosystems: Lessons from a suite of earth system models. *Frontiers in Marine Science*, 7. <https://doi.org/10.3389/fmars.2020.00698>
- Balwada, D., Smith, K. S., & Abernathy, R. (2018). Submesoscale vertical velocities enhance tracer subduction in an idealized Antarctic circumpolar current. *Geophysical Research Letters*, 45(18), 9790–9802. <https://doi.org/10.1029/2018GL079244>
- Barthélémy, S., Brajard, J., Bertino, L., & Counillon, F. (2022). Super-resolution data assimilation. *Ocean Dynamics*, 72(8), 661–678. <https://doi.org/10.1007/s10236-022-01523-x>
- Beech, N., Rackow, T., Semmler, T., Danilov, S., Wang, Q., & Jung, T. (2022). Long-term evolution of ocean eddy activity in a warming world. *Nature Climate Change*, 12(10), 910–917. <https://doi.org/10.1038/s41558-022-01478-3>
- Boer, G. J., & Arora, V. K. (2013). Feedbacks in emission-driven and concentration-driven global carbon budgets. *Journal of Climate*, 26(10), 3326–3341. <https://doi.org/10.1175/JCLI-D-12-00365.1>
- Bolton, T., & Zanna, L. (2019). Applications of deep learning to ocean data inference and subgrid parameterization. *Journal of Advances in Modeling Earth Systems*, 11(1), 376–399. <https://doi.org/10.1029/2018MS001472>
- Brett, G. J., Whitt, D. B., Long, M. C., Bryan, F. O., Feloy, K., & Richards, K. J. (2023). Submesoscale effects on changes to export production under global warming. *Global Biogeochemical Cycles*, 37(3), e2022GB007619. <https://doi.org/10.1029/2022GB007619>
- Bronslaer, B., Winton, M., Russell, J., Sabine, C. L., & Khatiwala, S. (2017). Agreement of CMIP5 simulated and observed ocean anthropogenic CO₂ uptake. *Geophysical Research Letters*, 44(24), 12212–298305. <https://doi.org/10.1002/2017GL074435>
- Bronslaer, B., & Zanna, L. (2020). Heat and carbon coupling reveals ocean warming due to circulation changes. *Nature*, 584(7820), 227–233. <https://doi.org/10.1038/s41586-020-2573-5>
- Bronslaer, B., Zanna, L., Munday, D. R., & Lowe, J. (2016). The influence of Southern Ocean winds on the North Atlantic carbon sink. *Global Biogeochemical Cycles*, 30(6), 844–858. <https://doi.org/10.1002/2015GB005364>
- Brown, P. J., McDonagh, E. L., Sanders, R., Watson, A. J., Wanninkhof, R., King, B. A., et al. (2021). Circulation-driven variability of Atlantic anthropogenic carbon transports and uptake. *Nature Geoscience*, 14(8), 571–577. <https://doi.org/10.1038/s41561-021-00774-5>
- Canadell, J., Monteiro, P., Costa, M., Cotrim da Cunha, L., Cox, P., Eliseev, A., et al. (2021). Global carbon and other biogeochemical cycles and feedbacks supplementary material [Book Section]. In V. Masson-Delmotte, et al. (Eds.), *Climate change 2021: The physical science basis. Contribution of working group I to the sixth assessment report of the intergovernmental panel on climate change*.
- Chang, P., Zhang, S., Danabasoglu, G., Yeager, S. G., Fu, H., Wang, H., et al. (2020). An unprecedented set of high-resolution earth system simulations for understanding multiscale interactions in climate variability and change. *Journal of Advances in Modeling Earth Systems*, 12(12), e2020MS002298. <https://doi.org/10.1029/2020MS002298>
- Chanut, J., Barrier, B., Large, W., Debreu, L., Penduff, T., Molines, J. M., & Mathiot, P. (2008). Mesoscale eddies in the Labrador Sea and their contribution to convection and restratification. *Journal of Physical Oceanography*, 38(8), 1617–1643. <https://doi.org/10.1175/2008JPO3485.1>
- Chassignet, E. P., & Marshall, D. P. (2008). Gulf Stream separation in numerical ocean models. *Ocean Modeling in an Eddy Regime*, 177, 39–61. <https://doi.org/10.1029/177GM05>
- Chassignet, E. P., & Xu, X. (2017). Impact of horizontal resolution (1/12° to 1/50°) on gulf stream separation, penetration, and variability. *Journal of Physical Oceanography*, 47(8), 1999–2021. <https://doi.org/10.1175/jpo-d-17-0031.1>
- Chen, H., Morrison, A. K., Dufour, C. O., & Sarmiento, J. L. (2019). Deciphering patterns and drivers of heat and carbon storage in the southern ocean. *Geophysical Research Letters*, 46(6), 3359–3367. <https://doi.org/10.1029/2018GL080961>
- Couespel, D. (2018). *La désoxygénation de l'océan au cours du 21ème siècle: influence des processus de petite et moyenne échelle* (Unpublished doctoral dissertation). Sorbonne Université.
- Couespel, D. (2023a). Stronger oceanic CO₂ sink in eddy-resolving simulations of global warming: Python scripts for model's output analysis and figure production [Software]. Zenodo. <https://doi.org/10.5281/zenodo.10278488>
- Couespel, D. (2023b). Stronger oceanic CO₂ sink in eddy-resolving simulations of global warming: Simulations outputs [Dataset]. Zenodo. <https://doi.org/10.5281/zenodo.10201158>
- Couespel, D., Lévy, M., & Bopp, L. (2021). Oceanic primary production decline halved in eddy-resolving simulations of global warming. *Biogeosciences*, 18(14), 4321–4349. <https://doi.org/10.5194/bg-18-4321-2021>
- Davila, X., Gebbie, G., Brakstad, A., Lauvset, S. K., McDonagh, E. L., Schwinger, J., & Olsen, A. (2022). How is the ocean anthropogenic carbon reservoir filled? *Global Biogeochemical Cycles*, 36(5), e2021GB007055. <https://doi.org/10.1029/2021GB007055>
- Delworth, T. L., Rosati, A., Anderson, W., Adcroft, A. J., Balaji, V., Benson, R., et al. (2012). Simulated climate and climate change in the GFDL CM2.5 high-resolution coupled climate model. *Journal of Climate*, 25(8), 2755–2781. <https://doi.org/10.1175/JCLI-D-11-00316.1>
- Delworth, T. L., & Zeng, F. (2008). Simulated impact of altered southern hemisphere winds on the Atlantic meridional overturning circulation. *Geophysical Research Letters*, 35(20), L20708. <https://doi.org/10.1029/2008GL035166>

- DeVries, T. (2014). The oceanic anthropogenic CO₂ sink: Storage, air-sea fluxes, and transports over the industrial era. *Global Biogeochemical Cycles*, 28(7), 631–647. <https://doi.org/10.1002/2013GB004739>
- du Plessis, M., Swart, S., Ansong, I. J., & Mahadevan, A. (2017). Submesoscale processes promote seasonal restratification in the Subantarctic Ocean. *Journal of Geophysical Research: Oceans*, 122(4), 2960–2975. <https://doi.org/10.1002/2016JC012494>
- Friedlingstein, P., Cox, P., Betts, R., Bopp, L., von Bloh, W., Brovkin, V., et al. (2006). Climate–carbon cycle feedback analysis: Results from the C4MIP model intercomparison. *Journal of Climate*, 19(14), 3337–3353. <https://doi.org/10.1175/JCLI3800.1>
- Friedlingstein, P., Jones, M. W., O’Sullivan, M., Andrew, R. M., Bakker, D. C. E., Hauck, J., et al. (2022). Global carbon budget 2021. *Earth System Science Data*, 14(4), 1917–2005. <https://doi.org/10.5194/essd-14-1917-2022>
- Fu, W., Moore, J. K., Primeau, F., Collier, N., Ogunro, O. O., Hoffman, F. M., & Randerson, J. T. (2022). Evaluation of ocean biogeochemistry and carbon cycling in CMIP earth system models with the International ocean model Benchmarking (IOMB) software system. *Journal of Geophysical Research: Oceans*, 127(10), e2022JC018965. <https://doi.org/10.1029/2022JC018965>
- Gent, P. R., & McWilliams, J. C. (1990). Isopycnal mixing in ocean circulation models. *Journal of Physical Oceanography*, 20(1), 150–160. [https://doi.org/10.1175/1520-0485\(1990\)020<0150:MIOCMj.2.0.CO;2](https://doi.org/10.1175/1520-0485(1990)020<0150:MIOCMj.2.0.CO;2)
- Gregory, J. M., Dixon, K. W., Stouffer, R. J., Weaver, A. J., Driesschaert, E., Eby, M., et al. (2005). A model intercomparison of changes in the Atlantic thermohaline circulation in response to increasing atmospheric CO₂ concentration. *Geophysical Research Letters*, 32(12). <https://doi.org/10.1029/2005GL023209>
- Gutjahr, O., Putrasahan, D., Lohmann, K., Jungclaus, J. H., Von Storch, J. S., Brüggemann, N., et al. (2019). Max planck institute earth system model (MPI-ESM1.2) for the high-resolution model intercomparison project (HighResMIP). *Geoscientific Model Development*, 12(7), 3241–3281. <https://doi.org/10.5194/gmd-12-3241-2019>
- Haarsma, R. J., Roberts, M. J., Vidale, P. L., Senior, C. A., Bellucci, A., Bao, Q., et al. (2016). High resolution model intercomparison project (HighResMIP v1.0) for CMIP6. *Geoscientific Model Development*, 9(11), 4185–4208. <https://doi.org/10.5194/gmd-9-4185-2016>
- Harrison, C. S., Long, M. C., Lovenduski, N. S., & Moore, J. K. (2018). Mesoscale effects on carbon export: A global perspective. *Global Biogeochemical Cycles*, 32(4), 680–703. <https://doi.org/10.1002/2017GB005751>
- Hauck, J., Zeising, M., Le Quéré, C., Gruber, N., Bakker, D. C. E., Bopp, L., et al. (2020). Consistency and challenges in the ocean carbon sink estimate for the global carbon budget. *Frontiers in Marine Science*, 7. <https://doi.org/10.3389/fmars.2020.571720>
- Henson, S. A., Laufkötter, C., Leung, S., Giering, S. L. C., Palevsky, H. I., & Cavan, E. L. (2022). Uncertain response of ocean biological carbon export in a changing world. *Nature Geoscience*, 15(4), 248–254. <https://doi.org/10.1038/s41561-022-00927-0>
- Hewitt, H., Fox-Kemper, B., Pearson, B., Roberts, M., & Klocke, D. (2022). The small scales of the ocean may hold the key to surprises. *Nature Climate Change*, 12(6), 496–499. <https://doi.org/10.1038/s41558-022-01386-6>
- Hirschi, J. J.-M., Barnier, B., Böning, C., Biastoch, A., Blaker, A. T., Coward, A., et al. (2020). The Atlantic meridional overturning circulation in high resolution models. *Journal of Geophysical Research: Oceans*, 125(4). <https://doi.org/10.1029/2019JC015522>
- Iudicone, D., Rodgers, K. B., Plancherel, Y., Aumont, O., Ito, T., Key, R. M., et al. (2016). The formation of the ocean’s anthropogenic carbon reservoir. *Scientific Reports*, 6(1), 35473. <https://doi.org/10.1038/srep35473>
- Jackson, L. C., Roberts, M. J., Hewitt, H. T., Iovino, D., Koenig, T., Meccia, V. L., et al. (2020). Impact of ocean resolution and mean state on the rate of AMOC weakening. *Climate Dynamics*, 55(7), 1711–1732. <https://doi.org/10.1007/s00382-020-05345-9>
- Jansen, M. F., Adcroft, A., Khani, S., & Kong, H. (2019). Toward an energetically consistent, resolution aware parameterization of ocean mesoscale eddies. *Journal of Advances in Modeling Earth Systems*, 11(8), 2844–2860. <https://doi.org/10.1029/2019MS001750>
- Karleskind, P., Lévy, M., & Mémerly, L. (2011). Modifications of mode water properties by sub-mesoscales in a bio-physical model of the North-east Atlantic. *Ocean Modelling*, 39(1), 47–60. <https://doi.org/10.1016/j.ocemod.2010.12.003>
- Katavouta, A., & Williams, R. G. (2021). Ocean carbon cycle feedbacks in CMIP6 models: Contributions from different basins. *Biogeosciences*, 18(10), 3189–3218. <https://doi.org/10.5194/bg-18-3189-2021>
- Krémeur, A. S., Lévy, M., Aumont, O., & Reverdin, G. (2009). Impact of the subtropical mode water biogeochemical properties on primary production in the North Atlantic: New insights from an idealized model study. *Journal of Geophysical Research*, 114(C), C07019. <https://doi.org/10.1029/2008JC005161>
- Kwiatkowski, L., Torres, O., Bopp, L., Aumont, O., Chamberlain, M., Christian, J. R., et al. (2020). Twenty-first century ocean warming, acidification, deoxygenation, and upper-ocean nutrient and primary production decline from CMIP6 model projections. *Biogeosciences*, 17(13), 3439–3470. <https://doi.org/10.5194/bg-17-3439-2020>
- Laufkötter, C., Vogt, M., Gruber, N., Aita-Noguchi, M., Aumont, O., Bopp, L., et al. (2015). Drivers and uncertainties of future global marine primary production in marine ecosystem models. *Biogeosciences*, 12(23), 6955–6984. <https://doi.org/10.5194/bg-12-6955-2015>
- Le Bras, I., Straneo, F., Muilwijk, M., Smedsrud, L. H., Li, F., Lozier, M. S., & Holliday, N. P. (2021). How much Arctic fresh water participates in the subpolar overturning circulation? *Journal of Physical Oceanography*, 51(3), 955–973. <https://doi.org/10.1175/JPO-D-20-0240.1>
- Lévy, M., Bopp, L., Karleskind, P., Resplandy, L., Ethé, C., & Pinsard, F. (2013). Physical pathways for carbon transfers between the surface mixed layer and the ocean interior. *Global Biogeochemical Cycles*, 27(4), 1001–1012. <https://doi.org/10.1002/gbc.20092>
- Lévy, M., Iovino, D., Resplandy, L., Klein, P., Madec, G., Treguier, A.-M., et al. (2012). Large-scale impacts of submesoscale dynamics on phytoplankton: Local and remote effects. *Ocean Modelling*, 43(44), 77–93. <https://doi.org/10.1016/j.ocemod.2011.12.003>
- Lévy, M., Klein, P., Treguier, A. M., Iovino, D., Madec, G., Masson, S., & Takahashi, K. (2010). Modifications of gyre circulation by sub-mesoscale physics. *Ocean Modelling*, 34(1), 1–15. <https://doi.org/10.1016/j.ocemod.2010.04.001>
- Lévy, M., Krémeur, A. S., & Mémerly, L. (2005). Description of the LOBSTER biogeochemical model implemented in the OPA system (Tech. Rep.). Laboratoire d’Océanographie Dynamique et de Climatologie - IPSL.
- Lique, C., & Thomas, M. D. (2018). Latitudinal shift of the Atlantic Meridional Overturning Circulation source regions under a warming climate. *Nature Climate Change*, 8(11), 1013–1020. <https://doi.org/10.1038/s41558-018-0316-5>
- Madec, G., Bourdallé-Badie, R., Bouffier, P.-A., Bricaud, C., Bruciaferri, D., Calvert, D., et al. (2017). NEMO ocean engine. Notes du Pôle de modélisation de l’Institut Pierre-Simon Laplace (IPSL). <https://doi.org/10.5281/ZENODO.1472492>
- Mahadevan, A., Tagliabue, A., Bopp, L., Lenton, A., Mémerly, L., & Lévy, M. (2011). Impact of episodic vertical fluxes on sea surface pCO₂. *Philosophical Transactions of the Royal Society A: Mathematical, Physical & Engineering Sciences*, 369(1943), 2009–2025. <https://doi.org/10.1098/rsta.2010.0340>
- Maier-Reimer, E., Mikolajewicz, U., & Winguth, A. (1996). Future ocean uptake of CO₂: Interaction between ocean circulation and biology. *Climate Dynamics*, 12(10), 711–721. <https://doi.org/10.1007/s003820050138>
- Mak, J., Maddison, J. R., Marshall, D. P., & Munday, D. R. (2018). Implementation of a geometrically informed and energetically constrained mesoscale eddy parameterization in an ocean circulation model. *Journal of Physical Oceanography*, 48(10), 2363–2382. <https://doi.org/10.1175/JPO-D-18-0017.1>

- Martínez-Moreno, J., Hogg, A. M., England, M. H., Constantinou, N. C., Kiss, A. E., & Morrison, A. K. (2021). Global changes in oceanic mesoscale currents over the satellite altimetry record. *Nature Climate Change*, *11*(5), 1–7. <https://doi.org/10.1038/s41558-021-01006-9>
- Nakano, H., Ishii, M., Rodgers, K. B., Tsujino, H., & Yamanaka, G. (2015). Anthropogenic CO₂ uptake, transport, storage, and dynamical controls in the ocean imposed by the meridional overturning circulation: A modeling study. *Global Biogeochemical Cycles*, *29*(10), 1706–1724. <https://doi.org/10.1002/2015GB005128>
- Oliver, E. C. J., O’Kane, T. J., & Holbrook, N. J. (2015). Projected changes to Tasman Sea eddies in a future climate. *Journal of Geophysical Research: Oceans*, *120*(11), 7150–7165. <https://doi.org/10.1002/2015JC010993>
- Rackow, T., Danilov, S., Goessling, H. F., Hellmer, H. H., Sein, D. V., Semmler, T., et al. (2022). Delayed Antarctic sea-ice decline in high-resolution climate change simulations. *Nature Communications*, *13*(1), 637. <https://doi.org/10.1038/s41467-022-28259-y>
- Resplandy, L., Lévy, M., & McGillicuddy, D. J., Jr. (2019). Effects of Eddy-Driven subduction on ocean biological carbon pump. *Global Biogeochemical Cycles*, *33*(8), 1071–1084. <https://doi.org/10.1029/2018GB006125>
- Ridge, S. M., & McKinley, G. A. (2020). Advective controls on the north Atlantic anthropogenic carbon sink. *Global Biogeochemical Cycles*, *34*(7), 1–17. <https://doi.org/10.1029/2019GB006457>
- Roberts, M. J., Hewitt, H. T., Hyder, P., Ferreira, D., Josey, S. A., Mizielinski, M., & Shelly, A. (2016). Impact of ocean resolution on coupled air-sea fluxes and large-scale climate. *Geophysical Research Letters*, *43*(19), 10430–10438. <https://doi.org/10.1002/2016GL070559>
- Roberts, M. J., Jackson, L. C., Roberts, C. D., Meccia, V., Docquier, D., Koenigk, T., et al. (2020). Sensitivity of the Atlantic meridional overturning circulation to model resolution in CMIP6 HighResMIP simulations and implications for future changes. *Journal of Advances in Modeling Earth Systems*, *12*(8), e2019MS002014. <https://doi.org/10.1029/2019MS002014>
- Roy, T., Bopp, L., Gehlen, M., Schneider, B., Cadule, P., Frölicher, T. L., et al. (2011). Regional impacts of climate change and atmospheric CO₂ on future ocean carbon uptake: A multimodel linear feedback analysis. *Journal of Climate*, *24*(9), 2300–2318. <https://doi.org/10.1175/2010JCLI3787.1>
- Ruan, X., Couespel, D., Lévy, M., Li, J., Mak, J., & Wang, Y. (2023). Combined physical and biogeochemical assessment of mesoscale eddy parameterisations in ocean models: Eddy induced advection at non-eddy-resolving resolutions. *Ocean Modelling*, *183*, 102204. <https://doi.org/10.1016/j.ocemod.2023.102204>
- Sallée, J.-B., Matear, R. J., Rintoul, S. R., & Lenton, A. (2012). Localized subduction of anthropogenic carbon dioxide in the Southern Hemisphere oceans. *Nature Geoscience*, *5*(8), 579–584. <https://doi.org/10.1038/ngeo1523>
- Sarmiento, J. L., Hughes, T. M. C., Stouffer, R. J., & Manabe, S. (1998). Simulated response of the ocean carbon cycle to anthropogenic climate warming. *Nature*, *393*(6), 245–249. <https://doi.org/10.1038/30455>
- Sarmiento, J. L., & Le Quéré, C. (1996). Oceanic carbon dioxide uptake in a model of century-scale global warming. *Science*, *274*(5291), 1346–1350. <https://doi.org/10.1126/science.274.5291.1346>
- Schwinger, J., Tjiputra, J. F., Heinze, C., Bopp, L., Christian, J. R., Gehlen, M., et al. (2014). Nonlinearity of ocean carbon cycle feedbacks in CMIP5 earth system models. *Journal of Climate*, *27*(11), 3869–3888. <https://doi.org/10.1175/JCLI-D-13-00452.1>
- Séférian, R., Berthet, S., Yool, A., Palmiéri, J., Bopp, L., Tagliabue, A., et al. (2020). Tracking improvement in simulated marine biogeochemistry between CMIP5 and CMIP6. *Current Climate Change Reports*, *6*(3), 95–119. <https://doi.org/10.1007/s40641-020-00160-0>
- Séférian, R., Nabat, P., Michou, M., Saint-Martin, D., Voldoire, A., Colin, J., et al. (2019). Evaluation of CNRM earth system model, CNRM-ESM2-1: Role of earth system processes in present-day and future climate. *Journal of Advances in Modeling Earth Systems*, *11*(12), 4182–4227. <https://doi.org/10.1029/2019MS001791>
- Sonnwald, M., Lguensat, R., Jones, D. C., Dueben, P. D., Brajard, J., & Balaji, V. (2021). Bridging observations, theory and numerical simulation of the ocean using machine learning. *Environmental Research Letters*, *16*(7), 073008. <https://doi.org/10.1088/1748-9326/ac0eb0>
- Spence, P., Saenko, O. A., Sijp, W., & England, M. H. (2013). North Atlantic climate response to Lake Agassiz drainage at coarse and ocean eddy-permitting resolutions. *Journal of Climate*, *26*(8), 2651–2667. <https://doi.org/10.1175/JCLI-D-11-00683.1>
- Swierczek, S., Mazloff, M. R., Morzfeld, M., & Russell, J. L. (2021). The effect of resolution on vertical heat and carbon transports in a regional ocean circulation model of the Argentine Basin. *Journal of Geophysical Research: Oceans*, *126*(7), e2021JC017235. <https://doi.org/10.1029/2021JC017235>
- Uchida, T., Balwada, D., Abernathey, R. P., McKinley, G. A., Smith, S. K., & Lévy, M. (2020). Vertical eddy iron fluxes support primary production in the open Southern Ocean. *Nature Communications*, *11*(1), 1–8. <https://doi.org/10.1038/s41467-020-14955-0>
- Uchiyama, Y., Suzue, Y., & Yamazaki, H. (2017). Eddy-driven nutrient transport and associated upper-ocean primary production along the Kuroshio. *Journal of Geophysical Research: Oceans*, *122*(6), 5046–5062. <https://doi.org/10.1002/2017JC012847>
- van Westen, R. M., & Dijkstra, H. A. (2021). Ocean eddies strongly affect global mean sea-level projections. *Science Advances*, *7*(15), eabf1674. <https://doi.org/10.1126/sciadv.abf1674>
- Wanninkhof, R. (1992). Relationship between wind speed and gas exchange over the ocean. *Journal of Geophysical Research*, *97*(C5), 7373–7382. <https://doi.org/10.1029/92JC00188>
- Winton, M., Anderson, W. G., Delworth, T. L., Griffies, S. M., Hurlin, W. J., & Rosati, A. (2014). Has coarse ocean resolution biased simulations of transient climate sensitivity? *Geophysical Research Letters*, *41*(23), 8522–8529. <https://doi.org/10.1002/2014GL061523>
- Yang, H., Lohmann, G., Krebs-Kanzow, U., Ionita, M., Shi, X., Sidorenko, D., et al. (2020). Poleward shift of the major ocean gyres detected in a warming climate. *Geophysical Research Letters*, *47*(5). <https://doi.org/10.1029/2019GL085868>
- Yeager, S., Castruccio, F., Chang, P., Danabasoglu, G., Maroon, E., Small, J., et al. (2021). An outsized role for the Labrador Sea in the multidecadal variability of the Atlantic overturning circulation. *Science Advances*, *7*(41), eabh3592. <https://doi.org/10.1126/sciadv.abh3592>
- Zanna, L., & Bolton, T. (2020). Data-driven equation discovery of ocean mesoscale closures. *Geophysical Research Letters*, *47*(17), e2020GL088376. <https://doi.org/10.1029/2020GL088376>